Proceedings of the International Gas Turbine Congress 2003 Tokyo
November 2-7, 2003

IGTC2003Tokyo TS-039

The Measurements of Unsteady Flow Field in an Axial Flow Fan Under Stalled Condition

Kwang-Ho KIM[1], You-Hwan SHIN[2], and Chang-Sik KANG[3]

[1] Thermal/Flow Control Research Center
Korea Institute of Science and Technology
P.O.Box 131, Cheongryang, Seoul 130-650, KOREA
Phone: +82-2-958-5681, FAX: +82-2-5689, E-mail: khkim@kist.re.kr
[2] Phone: +82-2-958-5586, FAX: +82-2-5689, E-mail: yhshin@kist.re.kr
[3] E-mail: class9@hanmail.net

ABSTRACT

This paper presents an experimental study on the fully developed rotating stall of an axial flow fan and unsteady flow in the blade passage. In this investigation, unsteady pressure was measured using high frequency pressure transducers mounted on the casing wall of rotor passage. The measurement of total pressure distributions upstream and downstream of the rotor blade passage were also carried out with specially designed high frequency total pressure probe. The signal was analyzed by FFT and Double Phase-Locked Ensemble Averaging Technique. From the results, a periodical behavior of the unsteady pressure field could be recognized and one period of rotating stall could be divided into three zones. The flow characteristics on each zone were described in detail and the pressure field was also analyzed in terms of the pressure distribution along pressure side and suction side on the blade tip profile.

NOMENCLATURE

bpf : blade passing frequency
frs : rotating stall frequency
fs : shaft frequency
N : number of sample or number of measured group
p_i : instantaneous pressure
p_t : total pressure
U : rotor tip speed
V_x, V_t: axial and tangential velocity
ΔP : pressure difference in the inlet and outlet of the rotor.
ϕ : flow coefficient
ρ_{air} : density of air
ψ : pressure coefficient

INTRODUCTION

Unsteady flow phenomena such as periodic rotating stall, which is one of the most serious instabilities, and broadband pressure fluctuation (Haupt et al., 1988) with non-periodic characteristics deteriorate the performance and stability of turbomachinery in vibration, noise and blade excitation. Thus, the mechanism of these unsteady phenomena is worth analyzing in the aspect of avoiding and inhibiting such instabilities. To understand and control the rotating stall, detail measurements and analysis on the structure of stall cell and flow characteristics inside stall cell are essentially required.

Larguier (1981) sketched the flow pattern in the stall cell by analyzing the unsteady pressure field measured on the casing wall of an axial compressor. Kato et al. (1995) and Poensgen et al. (1994) investigated the flow structure of the stall cell in a single stage axial compressor. Shiromi et al. (2000) studied the behavior of the stall cell by measuring unsteady pressure in the diagonal flow fan. And, Shin et al. (1999a) analyzed the flow characteristics within impeller blade passage in the centrifugal compressor under rotating stall.

In this study, measurements and analysis of unsteady pressure field on the casing wall and the variation of total pressure in span direction upstream and downstream of the rotor were conducted to understand the flow characteristics and structure of stall cell under rotating stall.

TEST FACILITY AND INSTRUMENTATION

An industrial axial flow fan, which has ten rotor blades of adjustable pitch type, was used as the test model in this study. These blades have a chord length of 138mm at hub and 107mm at tip. The rotor, which is driven by 11kW electric motor with a rotational speed of 1750rpm, has a tip clearance of 1.5mm and a hub to tip ratio of 0.5. The casing has inner diameter of 710mm. The system for unsteady pressure measurements on the casing wall consists of high frequency pressure transducer (Kulite, XCS-062), amplifier (Instruments Group, 2260), low pass filter (Kron-Hite, 3384), A/D Board (Data Translation, DT3003-PGL) and waveform analyzer (Analogic, D6500E). 13 High frequency pressure transducers were mounted on the casing wall of rotor passage as shown in Fig. 1. The total pressure was measured by traversing the single-hole unsteady pressure probe in span direction at p1 and p13. Here, the distance between each measuring point is 11mm and the p1 is positioned at 38.5mm upstream of the blade leading edge and 310mm downstream of the inlet bell-mouth. The p13 is positioned at 49.5mm apart from trailing edge.

The instantaneous pressure was collected at the sampling rate of 0.083msec (12kHz), which corresponds to 40 circumferential sampling points between one pitch of blade passage per one cycle. The reference signal for Phase Locked Averaging, which was installed at the position of 60 degree in circumferential direction from p1, also measured with the same sampling condition except being filtered with 100Hz.

In this investigation, Phase Locked Ensemble Averaging Technique (PLEAT), developed by Shin, were used for processing the measured signal. Details of measurement method and procedure

Manuscript Received on July 2, 2003

(a) Axial flow fan for test

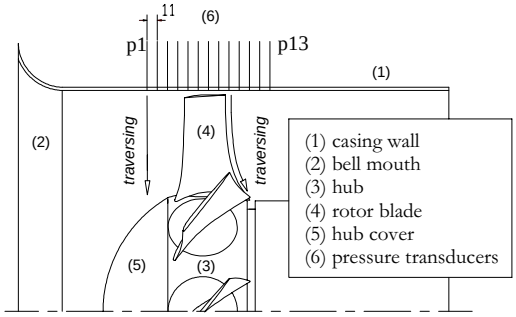

(b) Measurement positions

Fig. 1 Test facility and measurement positions

were described in (Shin et al., 1999b).

FAN CHARACTERISTICS

The characteristics of the test fan are shown in Fig. 2 (a). Flow coefficient (ϕ) and pressure coefficient (ψ) are defined as following equations (1) and (2).

$$\phi = \frac{V_x}{U} \tag{1}$$

$$\psi = \frac{\Delta p}{\rho_{air} U^2 / 2} \tag{2}$$

Figure 2 (b) shows the variation of two-dimensional velocity with various flow rates, which was measured along spanwise of the rotor by traversing 3-hole cobra probe at the measuring point, p13 in Fig. 1. Fig. 2 (c) indicates RMS (Root Mean Square) value of measured pressure fluctuation using high frequency pressure transducers on the casing wall at the position (p13). RMS value is defined as following equation (3).

$$RMS = \sqrt{\frac{1}{N}\sum_{i=1}^{N}(P_i - P_{mean})^2} \tag{3}$$

$$\text{(where, } p_{mean} = \sqrt{\frac{1}{N}\sum_{i=1}^{N} P_i}\text{)}$$

where, P_i is instantaneous pressure, and N means number of sample.

Figure 2 (d) shows the wall static pressure signals at p1 in the stable and unstable operating range and Fig. 2 (e) corresponds to their amplitude spectra. As shown in the characteristic curve of Fig. 2 (a), as the flow rate decreases further from ϕ = 0.412, both flow rate and pressure sharply drop at ϕ = 0.316. At this time, as shown in (b) and (c), tangential velocity and RMS value greatly increase. When flow rate is decreased further to ϕ = 0.262, the pressure is restored and RMS value decreases. As shown in the wall static pressure and its spectrum at ϕ = 0.389 in Fig. 2 (c) and (d), the influence by blade passing dominates flow characteristics in stable

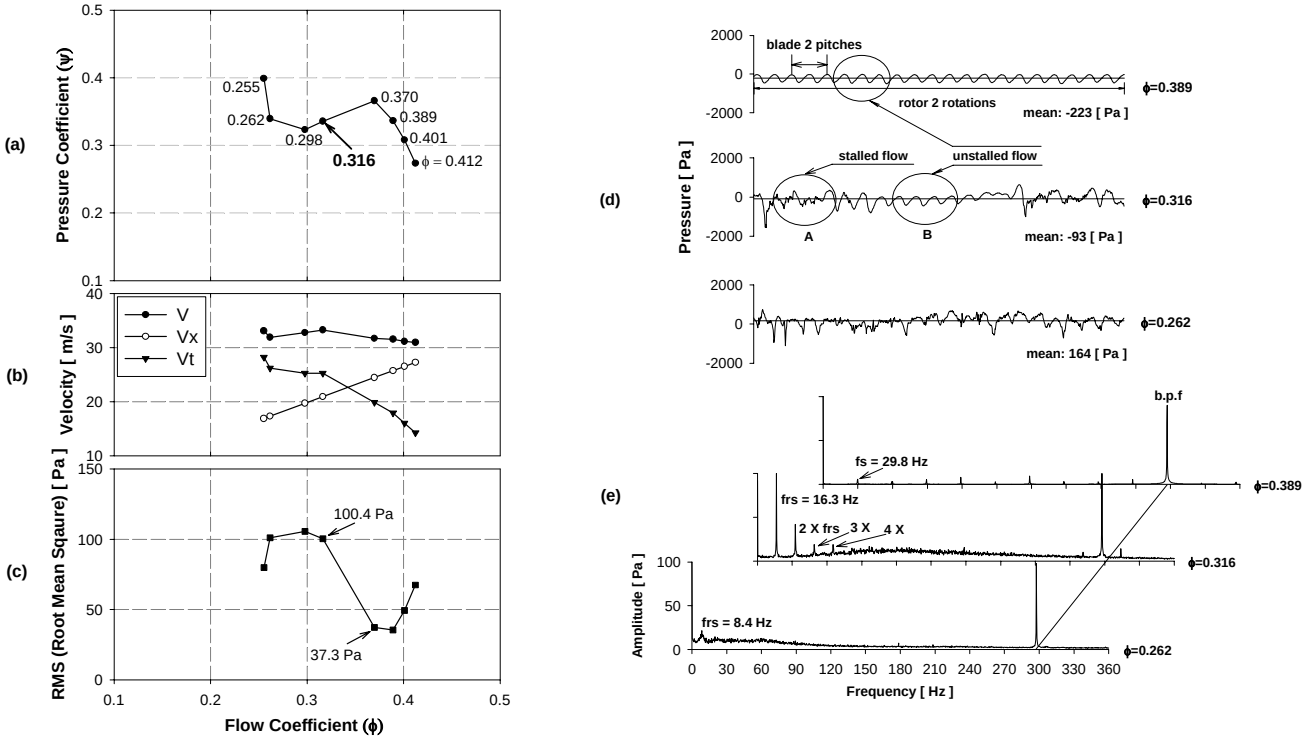

Fig. 2 (a) fan characteristics, (b) mean velocity variations (49.5mm downstream of the rotor), (c) RMS value of wall static pressure fluctuation (p13), (d) wall static pressure signals, and (e) pressure amplitude spectra

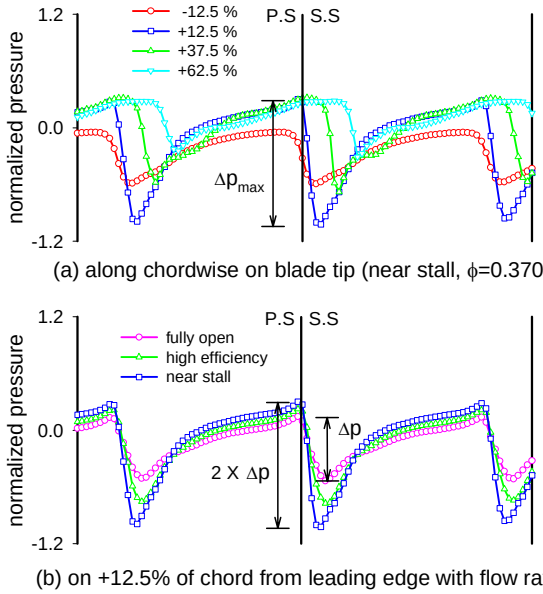

Fig. 3 Phase-averaged wall static pressure distributions

operating range.

The stalled flow region is indicated as 'A' at ϕ = 0.316 as shown in (d) and the unstalled flow region indicated as 'B' shows the similar pressure pattern with the stable operating range, ϕ = 0.389. In the result of spectrum analysis, the components of rotating stall and its harmonic frequency except the blade passing frequency newly appeared. By such appearance of rotating stall accompanying the pressure fluctuation with large amplitude, the RMS value suddenly increases in this range. It is a factor of causing noise and vibration.

If flow rate is reduced further to ϕ = 0.262, the feature of whole signal is changed to the type of non-periodic random signal contrary to ϕ = 0.389 and ϕ = 0.316, and it involves broadband frequency spectrum. At this flow rate, the component of rotating stall exists as narrowband type in the broadband frequency and the amplitude suddenly decreases. As proved in the research by Haupt et al. (1988), such broadband pressure spectrum is due to reverse flow effect. In this range, the amplitude and propagation speed of stall cell abruptly decreases and as shown in (b), the RMS value also decreases.

FLOW INSTABILITY

Wall Static Pressure

Figure 3 shows the phase-averaged wall static pressure distributions, which is normalized by dynamic pressure as shown in the denominator of the equation (2). Figure 3 (a) indicates pressure distributions along chordwise at the operation point near stall (ϕ =0.370) and (b) corresponds to those at 12.5% from blade leading edge with various flow rates. The pressure difference between the pressure and the suction side indicates the maximum value near the leading edge of the fan blade along chordwise. As the flow rate decreases to the operation point near stall, the pressure difference at 12.5% downstream from the blade leading edge gradually increases and reaches to about two times of that at maximum flow rate. The pressure difference in a blade passage leads to leakage flow through the blade tip clearance and flow instability can be caused by its development (Lakshminarayana, 1982, 1996).

Figure 4 illustrates the contours of RMS value for the wall static pressure at various flow rates. The RMS value can be defined by changing time mean value of the pressure in the previous equation (3), p_{mean}, into phase-averaged value.

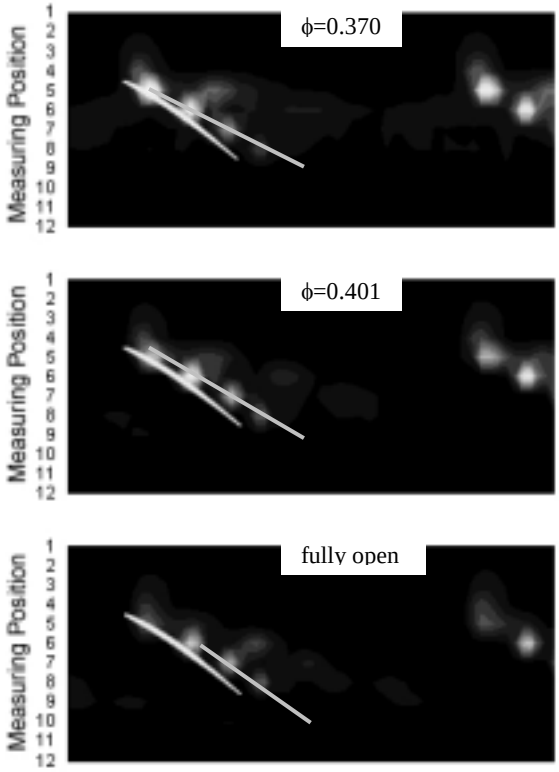

Fig. 4 RMS contour maps of static pressure on the casing wall with flow rate

The RMS values are relatively very large at the suction side of the blade, which are denoted by white color zone in the plot. As the flow rate decreases, they are gradually increased and move toward the blade leading edge. This means that the tip vortex is intensified, which is due to increase of the pressure difference.

Consequently as the flow rate is reduced to near stall onset point, intensity of the tip vortex due to leakage flow develops further and the flow instability is also increased. The similar result was reported in other investigation (Hoying et al., 1999).

Total Pressure Measurement

Figure 5 shows total pressure distributions with flow rate, which were measured at 4mm downstream of the rotor with flow rate. Whereas there are no remarkable differences with flow rate in the distributions of the total pressure at mid-span and hub, some noticeable effects are observed near tip region.

From Fig. 5 (a), which is corresponded to the result measured at 15mm from blade tip, as the flow rate is decreased toward near stall onset (ϕ = 0.370), the total pressure near the pressure side of the blade steeply increases while the loss of the total pressure near the suction side relatively grows and expands. Therefore high blade loading is generated in each blade passage.

It is considered that the generation of low total pressure zone near tip is due to the leakage interaction caused by mixing with the main flow. This interaction zone can be extended to about 15-20% of the blade span (Lakshminarayana, 1996).

Figure 6 shows time mean distributions of the total pressure in span direction upstream and downstream the rotor at flow rates corresponding to near stall (ϕ =0.370) and under stall condition (ϕ =0.316) respectively.

As shown in Fig. 6 (a), considering that the measured position is inlet of the rotor, it can be observed that the reverse flow of high-pressure zone exists near the tip upstream the rotor and high-pressure loss zone exists between 10% and 50% of blade span under stall condition. This result is because incoming flow is forced

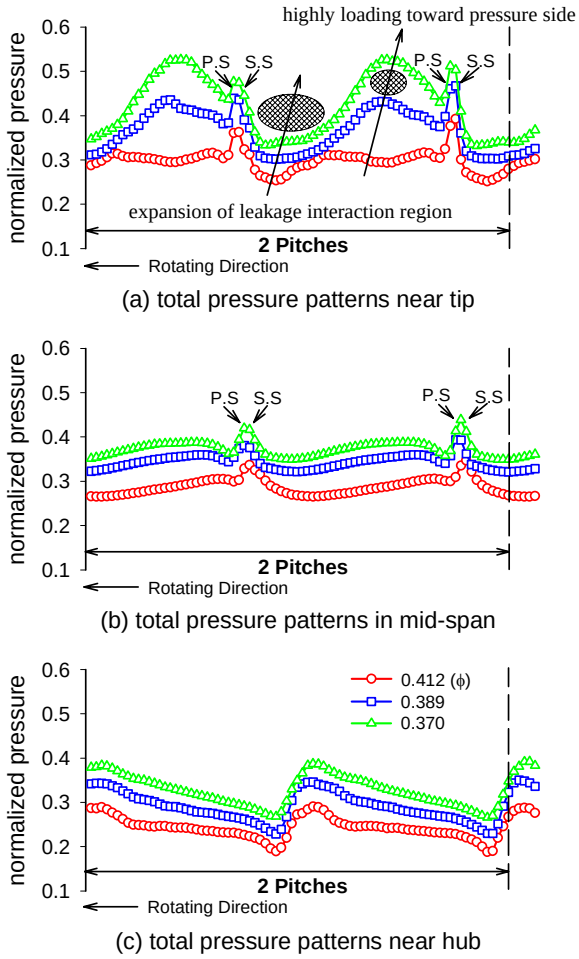

Fig. 5 Total pressure distributions along spanwise at 4mm downstream of the rotor

toward hub due to the blockage effect of stall cell near the casing, therefore the very low momentum flow zone is locally created between the blocked zone (the zone interacted by incoming flow and reverse flow near the casing) and incoming flow at mid-span. Consequently, this low momentum flow results in high-pressure loss.

The incoming flow between mid-span and hub, passed through the rotor inlet, is accelerated toward the casing downstream the rotor and relatively low absolute velocity in mid-span in order to preserve the mass conservation in the rotor inlet and outlet. Therefore, as shown in Fig. 6, the high-pressure zone is located near the tip and the large pressure loss zone is distributed in the mid-span.

Figure 7 (b)~(e) show the phase averaged pressure patterns for instantaneous total pressure signals upstream and downstream the rotor (measuring position p1 and p13 depicted in Fig. 1) at various positions in blade span direction and Fig. 7 (a) is result of wall static pressure measurements on the casing wall at rotor inlet (p1) and outlet (p13).

As shown in the Fig. 7 (b)~(e), The results clearly show that two regions, which is unstalled and stalled flow region observed in the result of wall static pressure measurements, exist in one period of rotating stall and repeats periodically.

In Fig. 7 (b), considering that the measured position is inlet of the rotor, it can be clearly observed that the stalled flow region is accompanied by strong reverse flow effect with high total pressure zone.

As shown in Fig. 7 (c), in comparison with the result at rotor inlet, it is observed that stalled flow region enlarges in circumferential direction at rotor outlet. Also, the mean pressure level and pressure

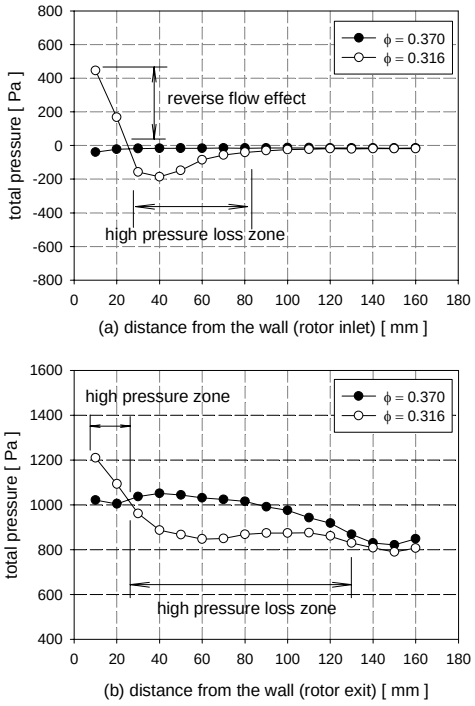

Fig. 6 Total pressure distributions at rotor inlet (a) and outlet (b) near stall (ϕ=0.370) and stall (ϕ=0.316) conditions

fluctuation in stalled flow region is relatively high compared to that of unstalled flow region.

Figure 7 (c)~(e) show that stalled flow region is reduced in circumferential direction at mid-span compared to the result at tip. The effect of stall cell almost disappears at hub.

In Fig. 7 (d), it is observed that the mean pressure level of unstalled flow region is higher than that of stalled flow region. This shows the opposite trend in comparison with the result at tip of Fig. 7 (c).

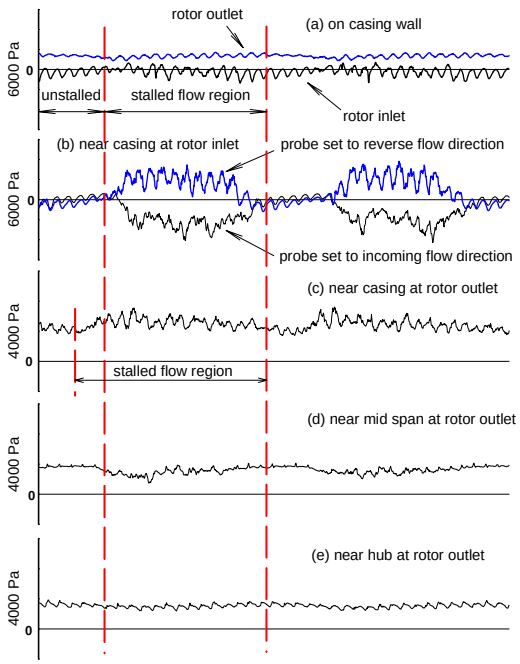

Fig. 7 Double phase-averaged static and total pressure distributions along spanwise at ϕ=0.316

Total Pressure Field Under Stall Condition

Figure 8 (a) and (b) illustrate total pressure fields at 38.5mm upstream of rotor blade leading edge and at 49.5mm downstream of the trailing edge respectively, which were plotted for two periods of the rotating stall. They are divided into two zones, stalled and unstalled flow region. The stalled flow region can be also divided into two zones, which denote bubbled and disturbed region (Kim et al., 2002).

In Fig. 8 (a), the effect of reverse flow is observed at stalled flow region of the tip and pressure loss zone locally exists between the tip and the mid-span. At downstream of the rotor, the stalled flow region near tip and the total pressure loss zone are developed respectively. The existence of the pressure loss zone at inlet of the rotor coincides with Poensgen's investigation (1994), which was measured by hot-wire probe. In this study, it is also observed at rotor exit and has the similar flow structure with that at inlet.

CONCLUSIONS

The instantaneous measurements of wall static pressure and total pressure at inlet and outlet of the rotor blade were performed. From the measured unsteady flow fields, the characteristics of the rotating stall were discussed and they lead to the following conclusions.

1. As the flow rate decreases to near stall onset point, the static pressure difference between pressure and suction side of the blade gradually increases and is maximized near the blade leading edge. At the same time the intensity of the tip vortex due to leakage flow develops further and the flow instability is affected by it.
2. At the tip region, as the flow rate is decreased toward near stall onset, the total pressure at the pressure side strongly increases whereas the low total pressure zone is generated by leakage interaction caused by mixing leakage flow through the tip clearance with the main flow. Then high blade loading is generated in each blade passage.
3. While the stalled flow region was accompanied with strong reverse flow near the tip at the inlet of the rotor, the region at rotor outlet was slightly enlarged in circumferential direction compared to that of rotor inlet and it was reduced at mid-span.

REFERENCES

Haupt, U., Rautenberg, M., and Abdel-Hamid, A. N., 1988, "Blade Exitation by Broad-Band Pressure Fluctuations in a Centrifugal Compressor", ASME J. of Turbomachinery, Vol. 110, pp. 129-137.

Hongwei Ma and Haokang Jiang, 2001, "Three-Dimensional Turbulent Flow in The Tip Region of an Axial Compressor Rotor Passage at a Near Stall Condition", ASME TURBO EXPO 2001, 2001-GT-0331.

Hoying, D. A., Tan, C. S., Vo Huu Duc, and Greitzer, E. M., 1999, "Role of Blade Passage Flow Structures in Axial Compressor Rotating Stall Inception," ASME J. of Turbomachinery, Vol. 121, No. 4, pp. 735-742.

Kato, D., Hirose, E., Ichida, K., Outa E., and Chiba, K, 1995, "Numerical and Experimental Study on Deep Stall Cell Behavior in an Axial Compressor", 1995 Yokohama International Gas Turbine Congress", 95-YOKOHAMA-IGTC-25, pp. II-173-180.

Kim, K. H., Shin, Y. H., and Kang, C. S., 2002, "A Study on the Unsteady Flow Phenomena in an Axial Flow Fan," The 4th International Conference on Pumps and Fans, Beijing, China, pp. 368-373.

Lakshminarayana, B., Pouagare, M, and Davino, R, 1982, "Three-Dimensional Flow Field in the Tip Region of a Compressor Rotor Passage – Part II: Turbulence Properties," ASME J. of Engineering for Power, Vol. 104, pp. 772-782.

Lakshminarayana, B., 1996, "Fluid Dynamics and Heat Transfer of Turbomachinery," John Wiley & Sons, Inc.

Larguier, R., 1981, "Experimental Analysis Methods for Unsteady Flows in Turbomachines", ASME J. of Engineering for Power, Vol. 103, pp. 415-423.

Poensgen, C. A., and Gallus, H. E., 1994, "Rotating Stall in a Single Stage Axial Flow Compressor", ASME IGTI paper, 94-GT-210.

Shin, Y. H., and Kim, K. H., 1999a, "Discharge Flow of a Centrifugal Impeller in Unstable Operating Region, Part 2: Measurement Result", J. IGTC 99 Kobe TS-53, pp. 81-87.

Shin, Y. H., and Kim, K. H., 1999b, "Discharge Flow of a Centrifugal Impeller in Unstable Operating Region of Centrifugal, Part 1: Measurement Techniques", IGTC 99 Kobe TS-53, pp. 653-658.

Shiromi, N., Kaneko, K., and Setoguchi, T., 2000, "International Flow of High Specific-Speed Diagonal Flow Fan with Rotating Stall (Behavior of Stall Cell), The Sixth Asian International Conference on Fluid Machinery Proceedings, pp.19-30.

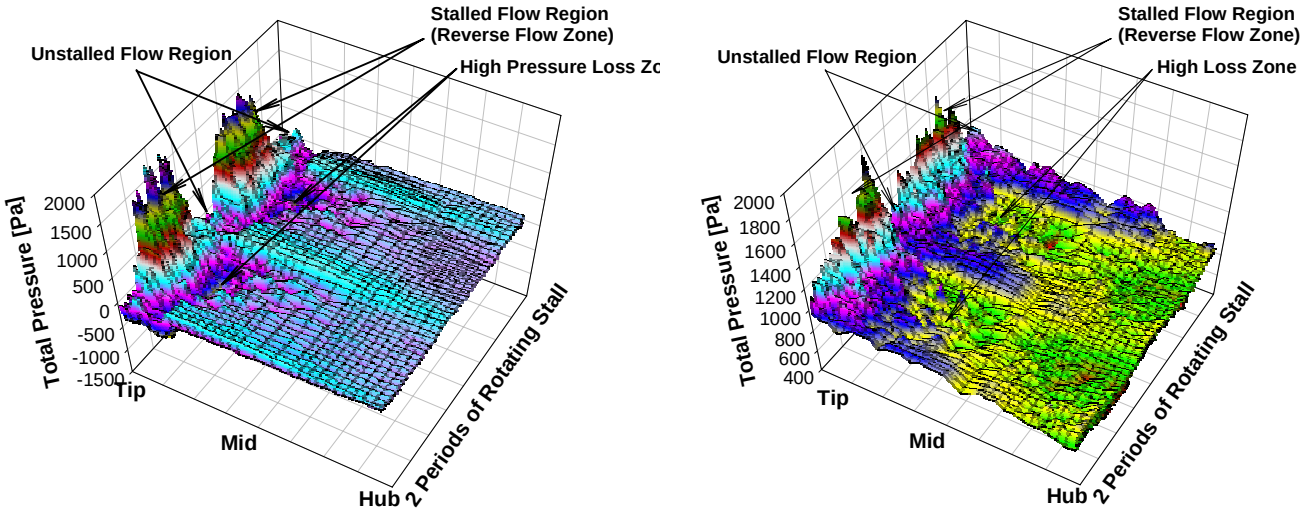

(a) 38.5mm rotor upstream

(b) 49.5mm rotor downstream

Fig. 8 Total pressure fields at rotor inlet and outlet under stall condition (ϕ=0.316)